Inter-individual differences in cell composition across the ventricular wall may explain variability in ECG response to serum potassium and calcium variations

Hassaan A Bukhari[1,2,3,4], Carlos Sánchez[1,4], Pablo Laguna[1,4], Mark Potse[2,3], Esther Pueyo[1,4]

[1]I3A, University of Zaragoza, IIS Aragón, Zaragoza, Spain
[2] Univ. Bordeaux, IMB, UMR 5251, Talence, France & [3] Carmen team, Inria Bordeaux – Sud-Ouest
[4] CIBER de Bioingeniería, Biomateriales y Nanomedicina, Instituto de Salud Carlos III, Spain

Abstract

Non-invasive monitoring of serum potassium ($[K^+]$) and calcium ($[Ca^{2+}]$) concentration can help to prevent arrhythmia in kidney patients. Current electrocardiogram (ECG) markers, including the T wave width (T_w) and its time-warped temporal morphological variability (d_w^U), correlate significantly with $[K^+]$ and $[Ca^{2+}]$ but these relations vary strongly between patients. We hypothesized that inter-individual differences in cell type distribution across the ventricular wall can explain this variability.

We computed T_w and d_w^U in simulated ECGs from a human heart-torso model at different proportions of endo-, mid-, and epicardial cells, while varying $[K^+]$ (3 to 6.2 mM) and $[Ca^{2+}]$ (1.4 to 3.2 mM). Electrical activity was simulated with a reaction-diffusion model with modified Ten Tusscher-Panfilov dynamics. Results were compared to data from 29 patients.

T_w and d_w^U correlated strongly with $[K^+]$ (absolute median Pearson coefficient $r = 0.70$ to 0.93) and $[Ca^{2+}]$ ($r = 0.69$ to 0.86) in simulations and in patients. Different cell type distributions reproduced inter-patient variability, with the same sign and magnitude of r.

In conclusion, the inter-patient variability in the relation between serum electrolytes and their ECG markers can indeed be explained by inter-individual differences in cell type distribution across the ventricular wall.

1. Introduction

Cardiovascular diseases including sudden cardiac death, myocardial infarction and other types of cardiac arrhythmias are the main cause of mortality among end-stage renal disease (ESRD) patients, accounting for 43% of deaths [1]. Most of these deaths are associated with abnormal potassium ($[K^+]$) and calcium ($[Ca^{2+}]$) levels, conditions known as hypo- or hyperkalemia and hypo- or hypercalcemia [2]. Maintenance and monitoring of normal electrolyte levels is therefore an important component in the treatment of ESRD patients.

Based on the reported effects of $[K^+]$ and $[Ca^{2+}]$ variations on the electrical activity of the heart, electrocardiogram (ECG) markers have been proposed for continuous monitoring of these electrolytes and subsequent application of timely therapies in ESRD patients. In particular, ECG markers quantifying characteristics of the T wave, representing ventricular repolarization in the ECG, have been shown to correlate with variations in $[K^+]$ and $[Ca^{2+}]$ [2].

Some of the proposed T wave markers evaluated durations and slopes of the T wave or portions of it [3]. In previous studies, we investigated T wave morphology markers by using time-warping and nonlinear dynamics techniques [4–6]. We observed large inter-patient variability in T wave morphology in response to $[K^+]$ and $[Ca^{2+}]$ variations [4–6]. Here, we hypothesized that evaluation of T wave morphology changes using human-specific torso models could provide relevant information on inter-individual repolarization characteristics. We quantified temporal morphological variability-based ECG repolarization features in whole-heart and torso models with different proportions of endocardial, midmyocardial and epicardial cells at varying $[K^+]$ and $[Ca^{2+}]$ and we compared simulation results to measurements in ESRD patients. We performed a sensitivity analysis to quantify the contribution of cell distributions in explaining inter-individual differences in T wave morphology at abnormal levels of $[K^+]$ and $[Ca^{2+}]$.

2. Methods

Study Design and Computational Modeling A human-specific heart and torso geometry was created from computed tomography data of a single patient [7]. The model included the ventricular wall with rule-based fiber orientation, ventricular and atrial cavities, torso surface, lungs, and an approximate anisotropic skeletal muscle layer. Cardiac activity was simulated with a reaction-diffusion model (200 µm resolution) using Ten

Tusscher–Panfilov dynamics [8] modified to adequately represent the relationship between action potential duration (APD) and $[Ca^{2+}]$ [9]. A total of 7 models with different proportions of endocardial, midmyocardial and epicardial cells were simulated, named $C136$, $C154$, $C316$, $C334$, $C352$, $C514$, $C532$. Here, Cxyz refers to a particular case, C, with x tens of endocardial, y tens of midmyocardial and z tens of epicardial cells in percentage terms (e.g. C136 represents the case with 10%, 30% and 60% of endo-, mid- and epicardial cells).

Simulations were run for four different values of $[K^+]$ (3, 4, 5.4, 6.2 mM), $[Ca^{2+}]$ (1.4, 2, 2.6, 3.2 mM) and their combinations ([3,3.2], [4,2.6], [5.4,2.0], [6.2,1.4] mM). These were selected to have similar values of $[K^+]$ and $[Ca^{2+}]$ as those observed in ESRD patients during hemodialysis (HD) [5, 6].

For each situation five beats were simulated. The initial state for each simulation was pre-calculated using a set of single cell simulations (one for each cell type), where the values of the model state variables after 1000 paced beats were considered as representative of the cell at steady state.

12-lead ECGs were computed with a lead-field method [10] using lead fields calculated in a 1-mm resolution finite-difference torso model. All simulations were performed on a cluster computer using a recent version of the Propag-5 software [10].

The simulated ECG signals were band-pass filtered (0.5-40 Hz) to remove baseline wander and possible high-frequency noise. A wavelet-based single-lead delineation method was used for QRS detection and wave delineation of each of the twelve leads [11]. To emphasize T wave components, principal components (PCs) were obtained by computing the auto-correlation matrix of the delineated T waves at the physiological value of $[K^+]$, i.e. 5.4 mM, and $[Ca^{2+}]$, i.e. 2 mM, in each model. The ECG recording was subsequently projected onto the direction of the first PC. The T waves in the first PC, which are the ones analyzed in this study, were delineated to compute their onsets, peaks and ends [11].

For comparative analysis, T waves in the first PC were obtained and delineated from ESRD patients [5]. The study population included 29 ESRD patients from Hospital Clínico Universitario de Zaragoza, Spain, from which 48-hour 12-lead ECGs were acquired.

T wave Morphology Characterization The following T wave descriptors were studied:

- T_w, representing the width of the T wave from T wave onset to T wave end;
- d_w^U, representing temporal variations in T wave morphology [4, 6, 12] (Figure 1).

d_w^U was computed with respect to a reference T wave, which was taken as the T wave calculated for the lowest $[K^+]$ when varying $[K^+]$ only, for the highest $[Ca^{2+}]$ when varying $[Ca^{2+}]$ only and for the lowest $[K^+]$ and highest $[Ca^{2+}]$ when varying $[K^+]$ and $[Ca^{2+}]$ simultaneously.

The descriptor d_w^U(Figure 1) quantifies the level of warping required to optimally align two T waves, reference, $\mathbf{f}^r(\mathbf{t}^r)$, and studied, $\mathbf{f}^s(\mathbf{t}^s)$, as briefly described in [4, 12]:

$$d_w^U = \frac{1}{N_r}\sum_{n=1}^{N_r} j\gamma^*(t^r(n)) \quad t^r(n)j, \tag{1}$$

where $\mathbf{t}^r = [t^r(1), ..., t^r(N_r)]^\top$ is the time interval of the reference T wave, N_r is the total duration of t^r and $\gamma^*(\boldsymbol{t}^r)$ is the function that optimally warps $\mathbf{f}^r(\mathbf{t}^r)$ into $\mathbf{f}^s(\mathbf{t}^s)$, being $\mathbf{t}^s = [t^s(1), ..., t^s(N_s)]^\top$ the time interval of the studied T wave. The optimal warping function, $\gamma^*(\boldsymbol{t}^r)$, was obtained using a dynamic programming algorithm (Figure 1, panel d). The warped T wave, $\boldsymbol{f}^s(\gamma^*(\boldsymbol{t}^r))$, is shown in Figure 1, panel b, together with the reference T wave, $\boldsymbol{f}^r(\boldsymbol{t}^r)$.

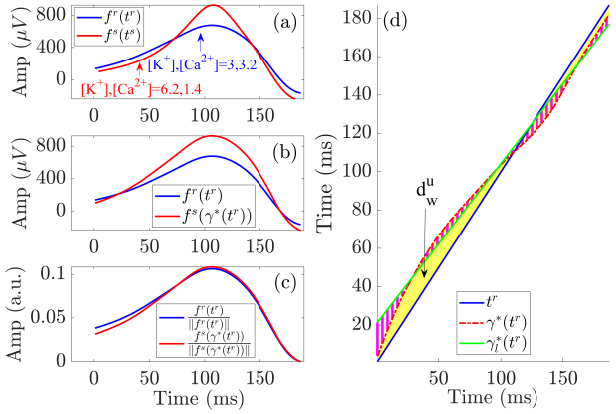

Figure 1. Time warping for a simulated T wave from a human heart-torso model (C154). Panel a: reference (blue) and studied (red) T waves aligned with respect to their gravity centers. Panels b–c: warped T waves before and after amplitude normalization. Panel d: computation of the marker d_w^U (yellow area).

Statistical Analysis Pearson correlation coefficient was computed to assess the strength of the linear relationship between T_w (d_w^U, respectively) and $[K^+]$ or $[Ca^{2+}]$.

Sensitivity analysis was performed to assess and quantify the contribution of different proportions of endocardial, midmyocardial and epicardial cells to inter-individual T wave variations at different $[K^+]$ and $[Ca^{2+}]$. For each T wave descriptor at each given concentration of $[K^+]$ and $[Ca^{2+}]$, measurements of the sensitivity ($S_{Y;c;a1;a2}$) to changes in the proportion of cells of each ventricular layer were computed as described in [4, 13]

3. Results and Discussion

Fig. 2 shows the relationship between T_{w} ($d_{\mathrm{w}}^{\mathrm{U}}$, respectively) and $[\mathrm{K}^+]$, $[\mathrm{Ca}^{2+}]$ and their combination in 3D simulations (panels a, c, e) and in patients (panels b, d, f). Panels a and b show T waves at different $[\mathrm{K}^+]$ and $[\mathrm{Ca}^{2+}]$. Tall and narrow peaked T waves were observed at high $[\mathrm{K}^+]$ in both simulated and patients' T waves, which led to lower T_{w} at higher simulated $[\mathrm{K}^+]$ (E_0) and at higher $[\mathrm{K}^+]$ at the start of the HD (h_0). This is illustrated for model C136 in panel c and for patient P10 in panel d and it is shown in average over models and patients in panels e and f, respectively. Regarding $d_{\mathrm{w}}^{\mathrm{U}}$, it was found to take the largest values at the highest $[\mathrm{K}^+]$ and lowest $[\mathrm{Ca}^{2+}]$ values in the simulations, which corresponded to the results obtained in patients at the start of the HD session (time point h_0) [4, 6]. These results indicated that elevated $[\mathrm{K}^+]$ and decreased $[\mathrm{Ca}^{2+}]$ led to enhanced T wave temporal morphological variability.

A correlation analysis was performed to assess the relationship between $[\mathrm{K}^+]$ or $[\mathrm{Ca}^{2+}]$ variations and the corresponding changes in T_{w} and $d_{\mathrm{w}}^{\mathrm{U}}$. Figure 3 illustrates the very strong linear Pearson correlation of $d_{\mathrm{w}}^{\mathrm{U}}$ with $[\mathrm{K}^+]$ and $[\mathrm{Ca}^{2+}]$ in the simulated cases (median value of 0.86 with $[\mathrm{K}^+]$ and 0.86 with $[\mathrm{Ca}^{2+}]$) and patients (median value of 0.93 with $[\mathrm{K}^+]$ and 0.84 with $[\mathrm{Ca}^{2+}]$). A strong association, even if lower than in the case of $d_{\mathrm{w}}^{\mathrm{U}}$, was observed between T_{w} and $[\mathrm{K}^+]$ or $[\mathrm{Ca}^{2+}]$ in both simulations (median value of 0.70 with $[\mathrm{K}^+]$ and 0.69 with $[\mathrm{Ca}^{2+}]$) and patients (median value of 0.93 with $[\mathrm{K}^+]$ and 0.79 with $[\mathrm{Ca}^{2+}]$).

Table 1. Results of the sensitivity analysis, $S_{Y;c;a_1;a_2}$, at different $[\mathrm{K}^+]$ and $[\mathrm{Ca}^{2+}]$, for varying proportions c of endocardial, midmyocardial or epicardial cells from minimum (a_1) to maximum (a_2) in each case.

$S_{Y;c;a_1;a_2}$	Y	T_{w}	$d_{\mathrm{w}}^{\mathrm{U}}$
c, a_1, a_2	$[\mathrm{K}^+]$, $[\mathrm{Ca}^{2+}]$ (mM)	%	%
Endo, 10, 50	$4.0, 2.6$	0.36	17.77
	$6.2, 1.4$	0.98	67.62
Mid, 10, 50	$4.0, 2.6$	6.40	14.32
	$6.2, 1.4$	4.56	43.50
Epi, 20, 60	$4.0, 2.6$	6.03	32.09
	$6.2, 1.4$	5.55	111.13

Table 1 shows the sensitivities of T_{w} and $d_{\mathrm{w}}^{\mathrm{U}}$ to variations in the proportion of endocardial, midmyocardial and epicardial cells at varying $[\mathrm{K}^+]$ and $[\mathrm{Ca}^{2+}]$. As can be observed from the table, $d_{\mathrm{w}}^{\mathrm{U}}$ was highly sensitive to variations in cell distributions, particularly under high $[\mathrm{K}^+]$ and low $[\mathrm{Ca}^{2+}]$ values. In particular, $d_{\mathrm{w}}^{\mathrm{U}}$ was increased for progressively larger proportions of epicardial cells, while it decreased for progressively larger proportions of endocardial or midmyocardial cells. Importantly, the sensitivity of $d_{\mathrm{w}}^{\mathrm{U}}$ to variations in cell distributions was enhanced at the highest $[\mathrm{K}^+]$ and lowest $[\mathrm{Ca}^{2+}]$ values, which could explain the remarkably larger inter-patient variability observed at the beginning of the HD, when $[\mathrm{K}^+]$ took the highest values and $[\mathrm{Ca}^{2+}]$ took the lowest values (see Fig. 2, panel f and Fig. 3). The largest sensitivity of $d_{\mathrm{w}}^{\mathrm{U}}$ was found to variations in the proportion of epicardial cells within the ventricular wall, which agrees with previous reports showing the contribution of epicardial cells to other forms of repolarization variability like T wave alternans [14]. For $[\mathrm{K}^+]$ = 6.2 mM and $[\mathrm{Ca}^{2+}]$ = 1.4 mM, sensitivity values above 110% were found, which corresponded to a coefficient of determination of 0.93.

4. Conclusions

A temporal morphological T wave marker, $d_{\mathrm{w}}^{\mathrm{U}}$, was highly correlated with varying $[\mathrm{K}^+]$ and $[\mathrm{Ca}^{2+}]$ in whole-heart and torso models, reproducing the relationship measured in ECGs from ESRD patients. The high inter-patient variability in $d_{\mathrm{w}}^{\mathrm{U}}$, particularly at high $[\mathrm{K}^+]$ and low $[\mathrm{Ca}^{2+}]$, was well replicated in simulations and was partly explained by differences in the proportions of endocardial, midmyocardial and epicardial cells, with the highest sensitivity found to variations in epicardial cells.

Acknowledgements

This work was supported by projects ERC-StG 638284 (ERC), PID2019-105674RB-I00 (Spain) and Marie Skłodowska-Curie grant 764738 (EU) and by European Social Fund (EU) and DGA through BSICoS group T39_20R and project LMP94_21. This work was granted access to the HPC resources of IDRIS under the allocation 2021-A0110307379 made by GENCI. M. Potse was supported by the French National Research Agency, grant reference ANR-10-IAHU04-LIRYC.

References

[1] Kanbay M, *et al.* Sudden death in hemodialysis: an update. Blood Purif 2010;30(2):135–145.

[2] Weiss JN, *et al.* Electrophysiology of hypokalemia and hyperkalemia. Circ Arrhythm Electrophysiol 2017;10(3).

[3] Pilia N, *et al.* Quantification and classification of potassium and calcium disorders with the electrocardiogram: What do clinical studies, modeling, and reconstruction tell us? APL Bioeng 2020;4(4):041501.

[4] Bukhari HA, *et al.* Characterization of T wave amplitude, duration and morphology changes during hemodialysis: Relationship with serum electrolyte levels and heart rate. IEEE Trans Biomed Eng 2021;68(8):2467–2478.

Figure 2. Panel a: Simulated T waves at varying $[K^+]$ (left), $[Ca^{2+}]$ (middle) and their combination (right) for a particular simulated case (C136). Panel b: T waves at varying $[K^+]$ and $[Ca^{2+}]$ for a particular patient (P10). Panels c and d: Variations in d_w^U and T_w at varying $[K^+]$ and $[Ca^{2+}]$ for the same simulated case and patient as in panels a and b. Panels e and f: Variations in the mean and median values of d_w^U and T_w at varying $[K^+]$ and $[Ca^{2+}]$ for all simulated cases (panel e) and all 29 patients during HD (panel f). Note: E_0 to E_3 correspond to different values of $[K^+]$ or $[Ca^{2+}]$ or their combination in simulated cases, with E_0 referring to the highest $[K^+]$ or/and lowest $[Ca^{2+}]$. h_0 to h_4 correspond to time points from HD start to HD end.

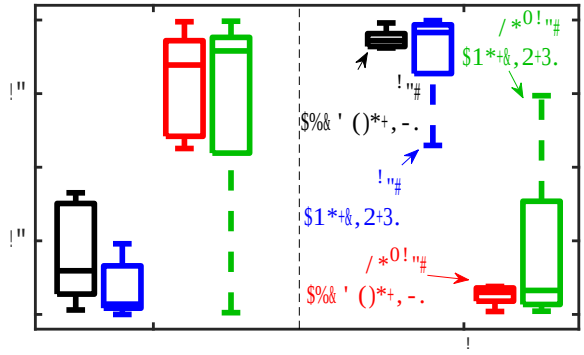

Figure 3. Box plots of Pearson correlation coefficients, r, between T_w (d_w^U respectively) and $[K^+]$ or $[Ca^{2+}]$ in simulations and patients.

[5] Bukhari HA, *et al.* Estimation of potassium levels in hemodialysis patients by T wave nonlinear dynamics and morphology markers. Comput Biol Med 2022;143:105304.

[6] Palmieri F, *et al.* Monitoring blood potassium concentration in hemodialysis patients by quantifying T-wave morphology dynamics. Sci Rep 2021;11(1):3883.

[7] Kania M, et al. Prediction of the exit site of ventricular tachycardia based on different ECG lead systems. In 2017 Computing in Cardiology (CinC). 2017; 1–4.

[8] Ten Tusscher KHWJ, *et al.* Alternans and spiral breakup in a human ventricular tissue model. Am J Physiol Heart Circ Physiol 2006;291(3):H1088–H1100.

[9] Severi S, *et al.* From in vivo plasma composition to in vitro cardiac electrophysiology and in silico virtual heart: the extracellular calcium enigma. Philos Trans A Math Phys Eng Sci 2009;367(1896):2203–2223.

[10] Potse M. Scalable and accurate ECG simulation for reaction-diffusion models of the human heart. Front Physiol 2018;9.

[11] Martínez JP, *et al.* A wavelet-based ECG delineator: evaluation on standard databases. IEEE Trans Biomed Eng 2004;51(4):570–581.

[12] Ramírez J, *et al.* Variability of ventricular repolarization dispersion quantified by Time-warping the morphology of the T-waves. IEEE Trans Biomed Eng 2017; 64(7):1619–1630.

[13] Romero L, *et al.* Impact of ionic current variability on human ventricular cellular electrophysiology. Am J Physiol Heart Circ Physiol 2009;297(4):H1436–1445.

[14] Janusek D, *et al.* The roles of mid-myocardial and epicardial cells in T-wave alternans development: a simulation study. Biomed Eng Online May 2018;17(1):57.